



## Environmentally assisted cracking resistance of Al–Cu–Li alloy AA2195 using slow strain rate test in 3.5% NaCl solution

R. GHOSH, A. VENUGOPAL, P. RAMESH NARAYANAN, S. C. SHARMA, P. V. VENKITAKRISHNAN

Materials and Metallurgy Group, Materials and Mechanical Entity, Vikram Sarabhai Space Centre,  
Thiruvananthapuram-695022, Kerala, India

Received 3 March 2016; accepted 29 June 2016

**Abstract:** The general corrosion and environmental cracking resistances of Al–Cu–Li alloy AA2195 were investigated in 3.5% NaCl environment and compared with those of another high strength alloy AA2219. The general corrosion resistance of these alloys was examined using immersion corrosion and potentiodynamic polarization tests, while the stress corrosion cracking (SCC) resistance was evaluated by slow strain rate test (SSRT) method. The tested samples were further characterized by SEM–EDS and optical profilometry to study the change in corrosion morphology, elemental content and depth of corrosion attack. The reduction in ductility was used as a parameter to evaluate the SCC susceptibility of the alloys. The results indicated that the corrosion resistance of AA2195 alloy was better than that of AA2219 alloy as it exhibited lower corrosion rate, along with lower pit depth and density. However, the SCC index ( $\epsilon_{\text{NaCl}}/\epsilon_{\text{air}}$ ) measured was greater than 0.90, indicating good environmental cracking resistance of both the alloys. Detailed fractography of the failed samples under SEM–EDS, in general, revealed a typical ductile cracking morphology for both the alloys.

**Key words:** Al–Cu–Li alloy; stress corrosion cracking; fractography; potentiodynamic polarization

### 1 Introduction

The Al–Cu–Li alloy AA2195 is used in the aerospace industry due to its light mass, high strength, good toughness and weldability. When compared with the conventional AA2219 alloy, this alloy offers an improved strength of 30%–40% and a reduction in density of 10% [1,2]. In view of the above advantages, this alloy has been considered as a replacement of AA2219 alloy for the fabrication of cryogenic propellant tanks. High strength of the alloy is achieved mainly by the precipitation of *T1* phases ( $\text{Al}_2\text{CuLi}$ ) after thermo-mechanical working followed by aging. Although the stress corrosion cracking (SCC) resistance of AA2219 alloy in T87 temper condition has been reasonably studied and found that the alloy exhibits good SCC resistance, similar studies on AA2195 have not yet studied and reported in detail. Limited results on the environmental cracking resistance of AA2195 alloy remain contradictory and vary depending on the aging temperature and the level of thermomechanical working. HU and MELETIS [3] compared the corrosion and SCC

resistance of AA2195 and AA2219 alloys using slow strain rate test (SSRT) and constant load (CL) test methods. Their study indicated that the alloy suffered SCC under SSRT conditions where the crack initiation was mostly from pitting. According to them, the mechanism of SCC was due to hydrogen absorption from the localized corrosion pits. They also reported that the SCC resistance of AA2195 was better than that of AA2219 alloy under the tested conditions. However, their results did not show the details of thermo-mechanical working and the aging temperature of the alloy tested for SCC. Similar high SCC susceptibility for weldalite 049 was reported by MOSHIER et al [4]. They compared two alloys with different Cu contents (5.30% and 4.80%, mass fraction) in which the alloy with higher Cu content failed by SCC. The lower Cu-containing alloy did not show SCC as it underwent severe pitting. The reason for the absence of SCC for the lower Cu-containing alloy was not explained in their work. Both the alloys were stretched to 3% followed by aging at 160 °C. In a recently reported work, WANG et al [5] examined the SCC resistance of AA2195 alloy by subjecting the alloy to different aging temperatures

(135–200 °C). Based on the SEM fracture morphology, they concluded that the alloy suffered lower SCC susceptibility at low aging temperatures than at high aging temperatures. They did not introduce any cold working prior to artificial aging.

The objective of the present investigation is to evaluate the environmentally assisted cracking behaviour of AA2195 alloy after subjecting the alloy to 7% cold working prior to artificial aging. The corrosion and SCC resistances of the alloy were comparatively studied with those of AA2219 alloy under the same temper condition in 3.5% NaCl solution.

## 2 Experimental

### 2.1 Materials

AA2195 alloy having nominal composition around Al–4.2Cu–1.1Li–0.35Mg–0.35Ag–0.15Zr–0.15Fe–0.10Si (mass fraction, %) was used in the form of rolled plates with thickness of approximately 4 mm. The plates were realized through series of thermomechanical treatments (forging followed by rolling) from as-cast and homogenized billets cast in vacuum induction melting furnace under inert atmosphere. The detail of the casting technique was discussed elsewhere in details [6–8]. These plates were then heat-treated to T87 temper (solution-treated at 500 °C for 0.5 h + quenching in water + 7% cold working followed by artificial aging at 146 °C for 30 h). Similarly, AA2219 alloy having nominal composition Al–5.95Cu–0.27Mn–0.1Zr–0.09V–0.06Ti–0.12Fe–0.05Si–0.02Zn (mass fraction, %) was used in the form of rolled plates in T87 temper (solution treated at 535 °C for 0.5 h + quenching in water + 7% cold working followed by artificial aging at 163 °C for 24 h). The tensile specimens were fabricated by cutting the specimen coupons in longitudinal as well as in transverse directions. Sub-scale flat rectangular specimens with effective gauge dimensions of 24 mm × 6 mm × 4 mm were used for stress corrosion cracking (SCC) tests after detailed radiographic examination and tested as per ASTM G 129.

### 2.2 Microstructures

For microstructural observations, the samples were sectioned and polished down to 5 μm alumina finish followed by etching in freshly prepared Keller's reagent (5 mL HNO<sub>3</sub>, 3 mL HCl, 2 mL HF, and 190 mL distilled water) and examined under an Olympus GS 71 optical microscope (Olympus America, Center Valley, PA) and a Carl Zeiss EVO–50 scanning electron microscope (SEM; Carl Zeiss, Oberkochen, Germany). The fractured samples were examined under a SEM to observe the change in the fracture morphology as a result of the

exposure to the NaCl environment.

### 2.3 Potentiodynamic polarization

The electrochemical corrosion of the alloys (AA2195 and AA2219) was evaluated through potentiodynamic polarization tests using a computer-controlled Zhaner IM6ex electrochemical workstation. Samples were taken from the rolling plane of both the alloys to make specimens with an area of 0.5 cm<sup>2</sup>. The corrosion behaviour of the samples was examined in 3.5% NaCl solution (mass fraction) prepared using reagent-grade NaCl salt and deionised water. The tests were carried out using a standard three-electrode setup with platinum as the counter electrode, saturated calomel electrode (SCE) as the reference electrode, and the test specimens as the working electrode. A scan rate of 0.5 mV/s was used. All the scans were started from a potential of 300 mV below the corrosion potential ( $\phi_{\text{corr}}$ ). Prior to the experiment, the samples were ground with SiC papers up to 1000-grit followed by cleaning in acetone and water.

### 2.4 Immersion corrosion test

Immersion corrosion was performed by subjecting AA2219-T87 and AA2195-T87 alloy specimens (35 mm × 35 mm × 4 mm) in 3.5% NaCl solution for 20 d. Before immersion, all the specimens were polished up to 1000-grit SiC paper followed by ultrasonic cleaning in acetone and water. After immersion test, the specimen surfaces were cleaned by dipping in chromic–phosphoric acid as per ASTM G1 to remove the corrosion products. The surface morphology of the specimens was analyzed using stereo microscopy and optical profilometry (NANOVEA, USA). With the assistance of Mountain software package, the parameters such as average pit depth and pit density were compared between the two alloys.

### 2.5 Slow strain rate test (SSRT)

Stress corrosion susceptibility of alloy AA2195 was evaluated by the SSRT method as per ASTM G129 standard at a strain rate of  $5 \times 10^{-7} \text{ s}^{-1}$  and the same was compared with that of AA2219 alloy. The tests were performed in 3.5% NaCl and air as the corrosive and reference environments, respectively. SSRT was performed using a CORTEST CERT tensile testing machine (CORTEST Inc., Willoughby, OH, USA). An acrylic container was served as a cell to hold the specimen in the environment. The gauge portion of the samples was polished using 600-grit SiC paper on all the sides to obtain a smooth surface. The average elongation of the specimen was measured by a pair of linear variable displacement transducers positioned on both sides of the specimen. Galvanic corrosion of the

specimen and the grip material was avoided by using silicone rubber sealant to coat the interface between the specimen and the grip portions. The ratio of elongation at failure in the corrosive environment (NaCl solution) to that in air  $\varepsilon_{\text{NaCl}}/\varepsilon_{\text{air}}$  was used as a measure to assess the SCC susceptibility.

### 3 Results and discussion

#### 3.1 Microstructures

The microstructures of AA2195 alloy for both longitudinal (L) and long transverse (LT) directions are presented in Fig. 1. It can be seen that the microstructure is typical of thermomechanically treated alloy with uniform distribution of particles aligned along the working direction. The absence of cast microstructure and the elongated grains indicates that the alloy has been processed well. Some coarse constituent particles (0.5–10  $\mu\text{m}$ ) are aligned along the working direction, which may be Cu-based and Al–Cu–Fe intermetallics [9,10]. These particles were mostly as  $T1$  ( $\text{Al}_2\text{CuLi}$ ),  $\theta'$  ( $\text{Al}_2\text{Cu}$ ) and some  $\text{Al}_7\text{Cu}_2\text{Fe}$  as reported in Refs. [11–13]. The microstructure also exhibits dynamically recrystallized grains between the fibrous structures, which is in good agreement with the results in Refs. [14,15]. Similar microstructures observed for AA2219 are presented in Fig. 2 corresponding to L and LT directions.

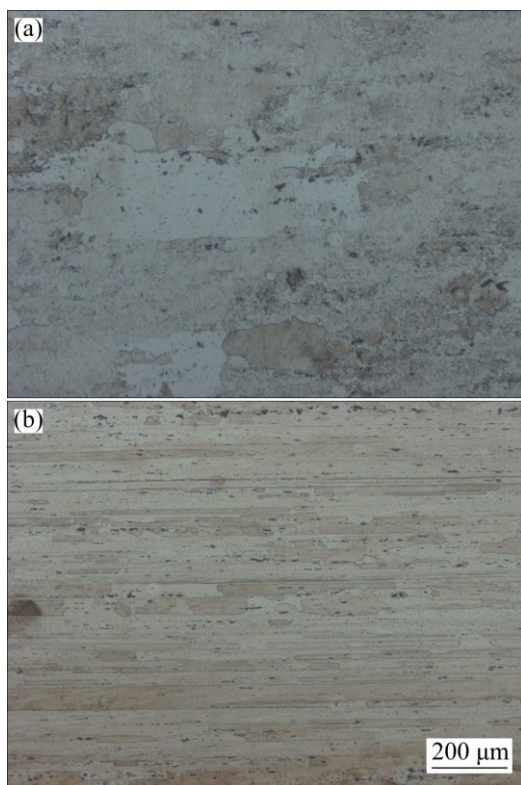


**Fig. 1** Optical micrographs of AA2195 alloy in longitudinal (a) and long transverse (b) directions

#### 3.2 Potentiodynamic polarization

Representative potentiodynamic polarization curves obtained for the aluminum alloys AA2195 and AA2219 are presented in Fig. 3. An examination of the polarization plots shows that the corrosion potential ( $\phi_{\text{corr}}$ ) of AA2219 alloy is nobler than that of AA2195 alloy. This can be attributed to the higher Cu content in AA2219 alloy than in AA2195 alloy [16,17]. Since Li is known to be more active, the  $\phi_{\text{corr}}$  of AA2195 alloy is lower than that of AA2219 alloy. The electrochemical parameters obtained from the polarization plots are shown in Table 1. It can be noted that the corrosion

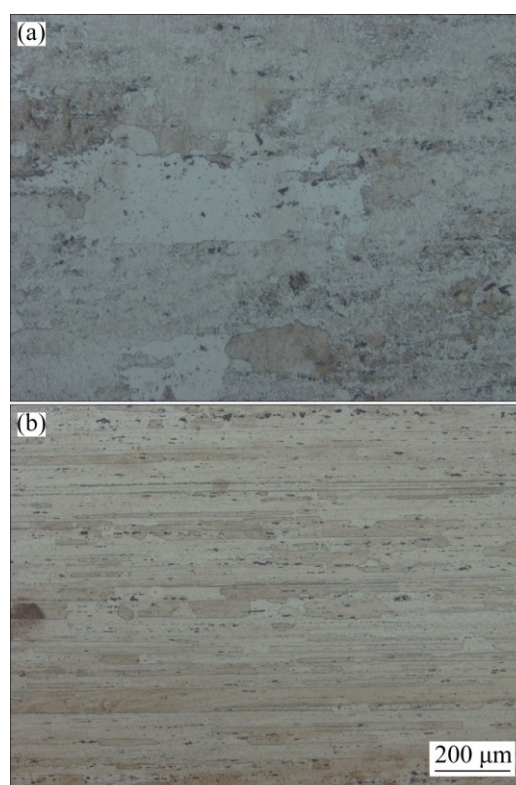


**Fig. 2** Optical micrographs of AA2219 alloy in longitudinal (a) and long transverse (b) directions

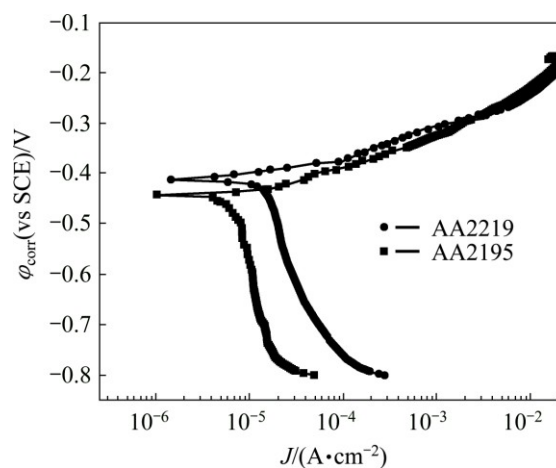


**Fig. 3** Potentiodynamic polarization curves obtained for AA2219 and AA2195 alloys in 3.5% NaCl solution

**Table 1** Electrochemical parameters obtained from polarization plots

Sample	$\varphi_{\text{corr}}$ (vs SCE)/V	$J_{\text{corr}}/(\mu\text{A}\cdot\text{cm}^{-2})$
AA2195-T87	-0.437	5.7
AA2219-T87	-0.397	12.0

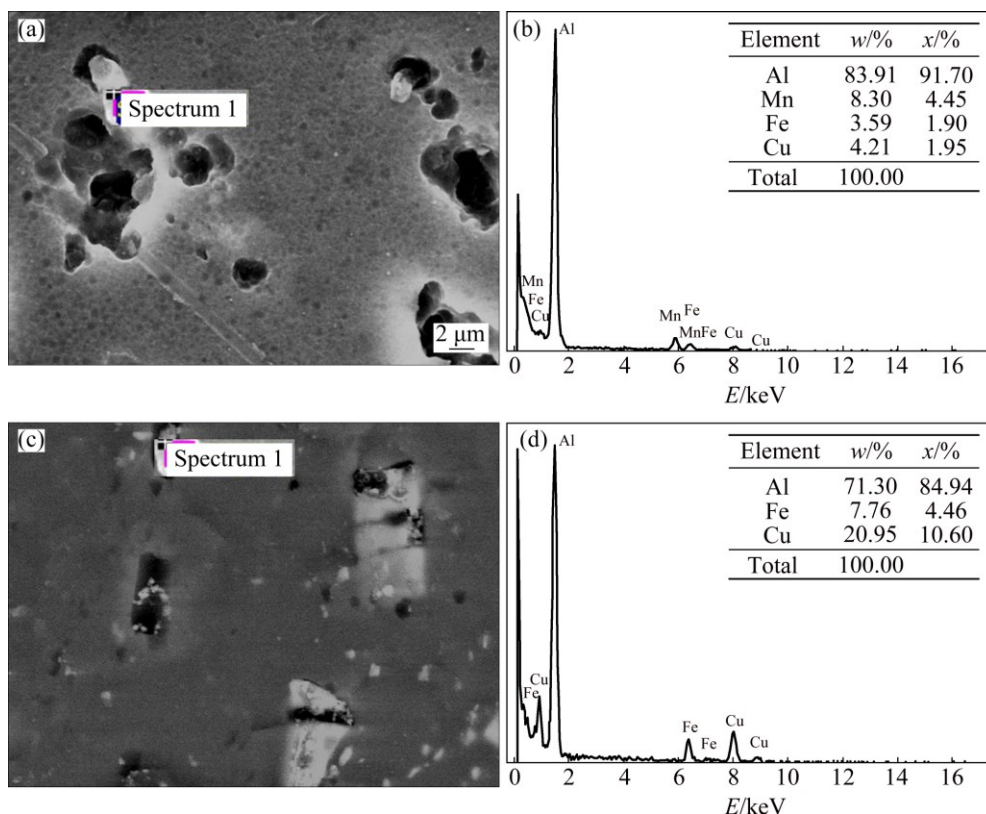
current density ( $J_{\text{corr}}$ ) is higher for AA2219 alloy than for AA2195 alloy. The absence of passivity for both the alloys suggests that pitting occurs spontaneously at the corrosion potential ( $\varphi_{\text{corr}}$ ) with increase in corrosion current. The higher rate of corrosion ( $J_{\text{corr}}$ ) measured for AA2219 alloy can be attributed to the increased cathodic reaction rates, as seen from the shift in the cathodic branch of the respective polarization curve. This can happen due to the higher amount of Cu in this alloy and the increase in oxygen reduction reaction over those phases during the corrosion reaction [18].

The corrosion morphologies of the samples observed under SEM after polarization tests are shown in Fig. 4. SEM-EDS spectra of Figs. 4(b) and (d) correspond to “Spectrum 1” in Figs. 4(a) and (c), respectively. The nature of attack was found to be similar for both the alloys as they suffered more localized corrosion where the corrosion pits initiated from second phase particles containing mostly Cu and Fe typical of 2000 series aluminum alloys. It can be noted that the corrosion attack was more intense on AA2219 alloy than on AA2195 alloy. Since Cu is nobler compared with

matrix aluminum, the aluminum matrix was corroded preferentially, leaving the Cu-rich phase which is evidently seen from the SEM image (Fig. 4(a)). In the case of AA2195 alloy, the Li-containing particles were corroded preferentially, thus protecting the matrix aluminum. The thick corrosion product on the particles showed that Li dissolved preferentially during the initial period of corrosion reaction and thereafter it may behave similar to  $\text{CuAl}_2$  phase as seen in the case of AA2219 alloy. Since Li analysis was not possible by SEM-EDS, the resulting elements are found to be only Cu and Fe (Fig. 4(b)).

### 3.3 Immersion corrosion test

The low magnification stereo images along with three dimensional (3D) optical profilometer images of AA2219 and AA2195 samples after immersion in 3.5% NaCl solution for 20 d are shown in Fig. 5. The stereo photographs (Figs. 5(a) and (b)) clearly show that the density of pits is higher for AA2219 alloy than for AA2195 alloy. The 2D profilometer images (Figs. 5(c) and (d)) clearly indicate that the depth of the pits is much higher for AA2219 alloy than for AA2195 alloy, shown by the scale alongside in Figs. 5(c) and (d) and the depth profile analysis in Figs. 5(e) and (f). This shows that the corrosion resistance of AA2195 alloy is better than that of AA2219 alloy. The polarization test results showed higher corrosion rate for AA2219 alloy than for AA2195

**Fig. 4** SEM images (a,c) and EDS spectra (b, d) of potentiodynamic polarized samples of AA2219-T87 (a, b) and AA2195-T87 (c, d)

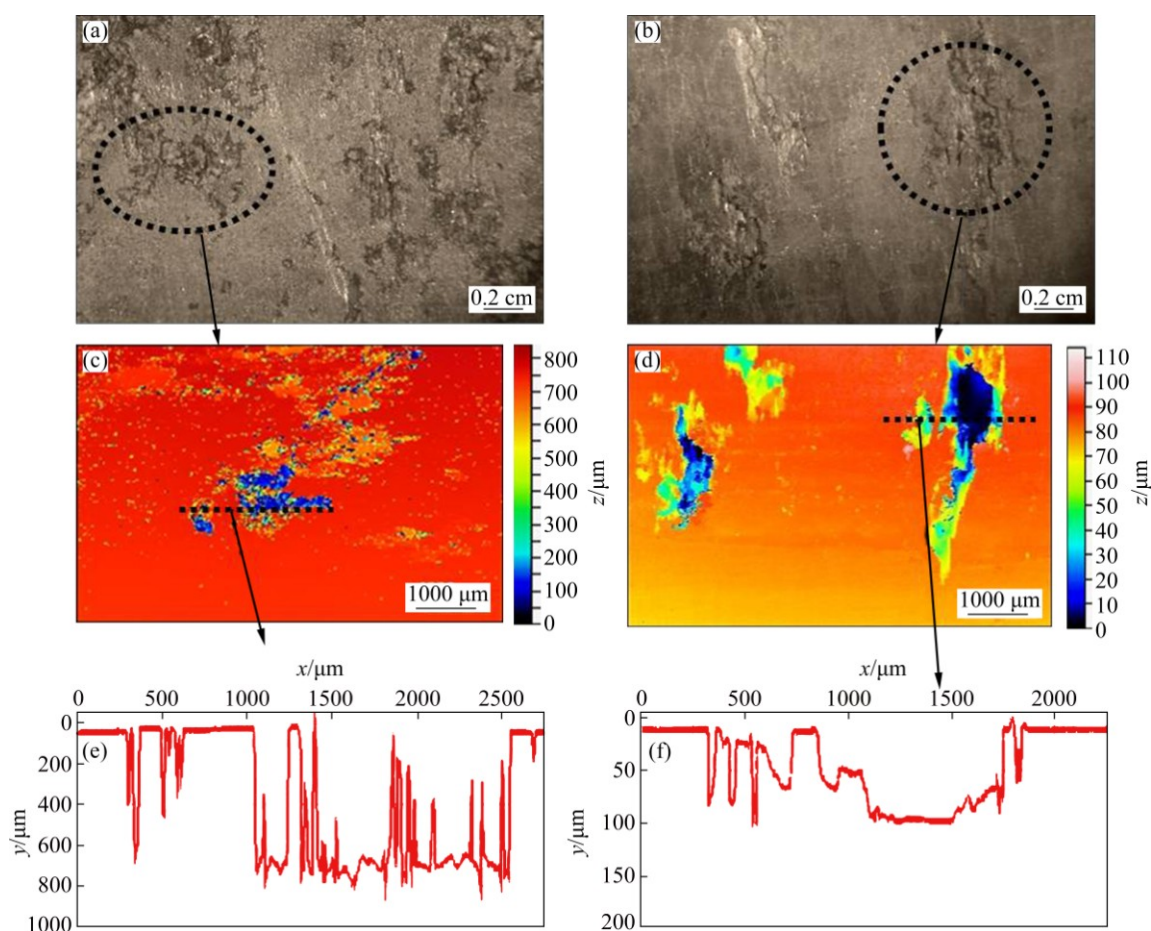


**Fig. 5** Typical stereo and optical profilometry images showing extent of corrosion for AA2219 (a) and AA2195 (b) alloy after immersion in 3.5% NaCl for 20 d

alloy. The better corrosion resistance of AA2195 alloy could be due to the presence of Li which enhances the passive film formation on the alloy [3]. The comparison of the microstructure of these alloys and the nature of attack after immersion test revealed that both alloys exhibited a kind of localized corrosion in which the corrosion reactions are controlled not only by the size and distribution of second phase particles but also the electrochemical nature of the particles.

### 3.4 Slow strain rate tests (SSRT)

Figures 6 and 7 show the stress–strain curves obtained for AA2195 and AA2219 aluminum alloys, respectively. The SSRT data such as UTS, elongation and SCC index measured from the stress–strain plots for both alloys are summarized in Table 2. An examination of the stress–strain plots showed that the ductility of the samples was not affected significantly as a result of exposure to environment. The UTS values for AA2195 alloy are much higher than those for AA2219 alloy, which gives a clear indication of the effect of T1 ( $\text{Al}_2\text{CuLi}$ ) precipitates which impart higher strengthening

for the alloy, whereas such effect is seen on AA2219 alloy which gets strengthened by the precipitation of  $\theta'$  ( $\text{Al}_2\text{Cu}$ ) particles [19,20]. The sole reason for why AA2195 alloy is the candidate material for replacing AA2219 alloy in propellant tanks is its high specific strength [21,22]. In this study, SCC index ( $\epsilon_{\text{NaCl}}/\epsilon_{\text{air}}$ ) was used to evaluate the SCC resistance of all the samples, which is the ratio of the elongation of the samples tested in 3.5% NaCl solution and air. The greater the SCC index value is, the better the SCC resistance is. An index value of unity implies that the material exhibits no SCC susceptibility. The measured SCC index values for both alloys are summarized in Table 2. It can be noted that the SCC index values are close to 1 for AA2195 alloy in both longitudinal and long transverse directions, indicating good SCC resistance. Similarly, AA2219 alloy is also found to have similar values for the samples tested in longitudinal and long transverse directions. This shows that the environmental cracking resistances of both the alloys are comparable in 3.5% NaCl solution and for the strain rate used in the present study. However, significant improvement in the strength values for

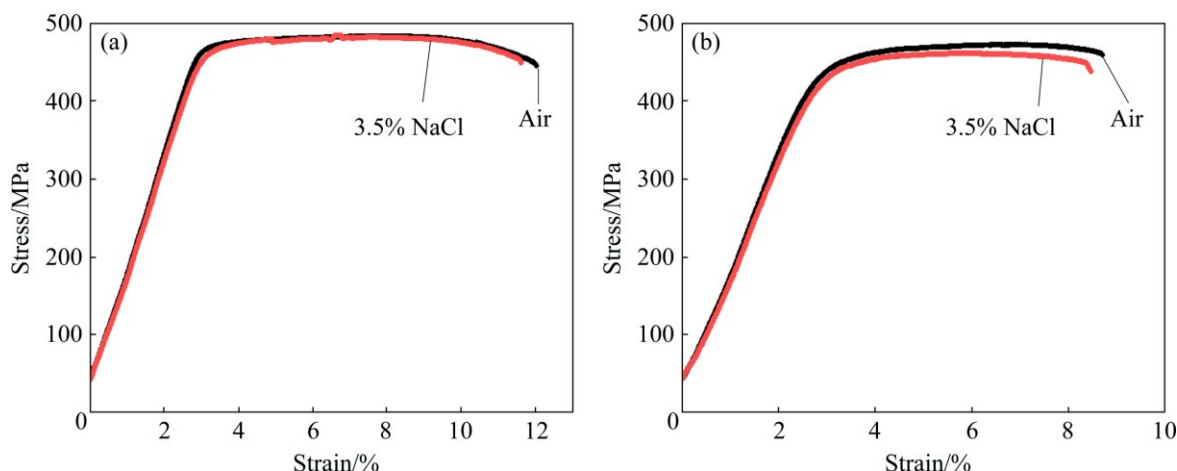


**Fig. 6** Stress–strain plots obtained for AA2195-T87 alloy tested in longitudinal (a) and long transverse (b) directions in 3.5% NaCl solution and air

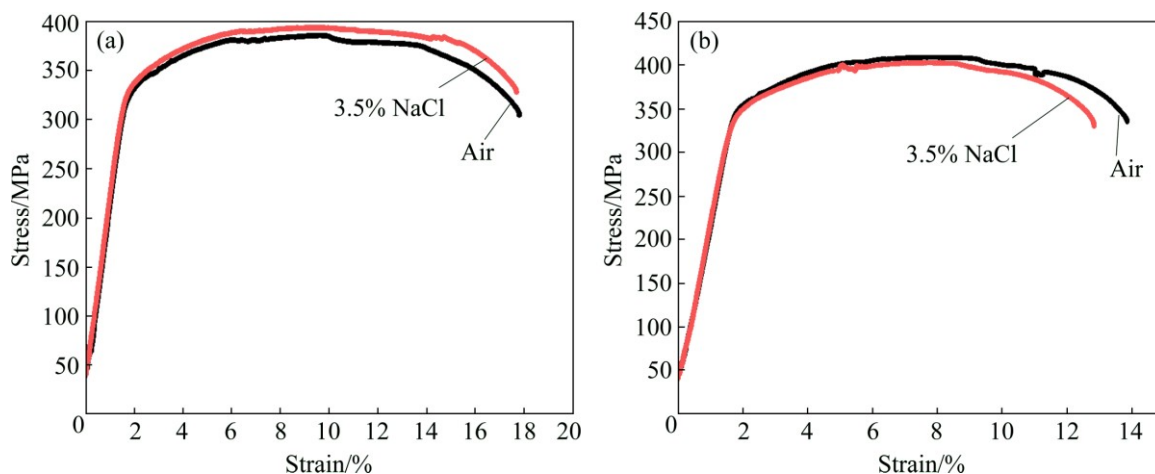


**Fig. 7** Stress–strain plots obtained for AA2219-T87 alloy tested in longitudinal (a) and long transverse (b) directions in 3.5% NaCl solution and air

**Table 2** Mechanical parameters of alloys obtained from SSRT tests in 3.5% NaCl solution and air

Sample	Environment	UTS/MPa	Elongation/%	SCC index
AA2195-T87(L)	Air	481	12.0	0.98
	NaCl	480	11.7	
AA2195-T87(LT)	Air	480	9.0	0.98
	NaCl	478	8.8	
AA2219-T87(L)	Air	383	18.0	0.97
	NaCl	392	17.6	
AA2219-T87(LT)	Air	409	14.0	0.93
	NaCl	397	13.0	

AA2195 alloy is very important for increasing the rocket payload capabilities. An examination of the fracture surfaces observed under SEM after SSRT revealed a typical ductile cracking morphology for both air and NaCl environment tested samples, as shown in Figs. 8

and 9. This confirms the absence of SCC susceptibility of these two kinds of aerospace aluminum alloys under slow strain rate conditions.

The above results revealed that AA2195 alloy exhibited lower corrosion rate than AA2219 alloy, indicating good general corrosion resistance of AA2195 alloy. This was due to the electrochemical nature of the strengthening phases on these alloys resulting in less number of localized pits and lower depth of attack on AA2195 alloy. These results are in agreement with the published data on the corrosion resistance of AA2195 alloy. However, comparing the environmental cracking resistance of the alloy with the published data, the present study clearly showed high environmental cracking resistance based on the SSRT results and the fracture morphology observations. While the reported results indicated high susceptibility of AA2195 alloy. Good SCC resistance of the alloy obtained in the present study is due to the absence or inadequate cold working

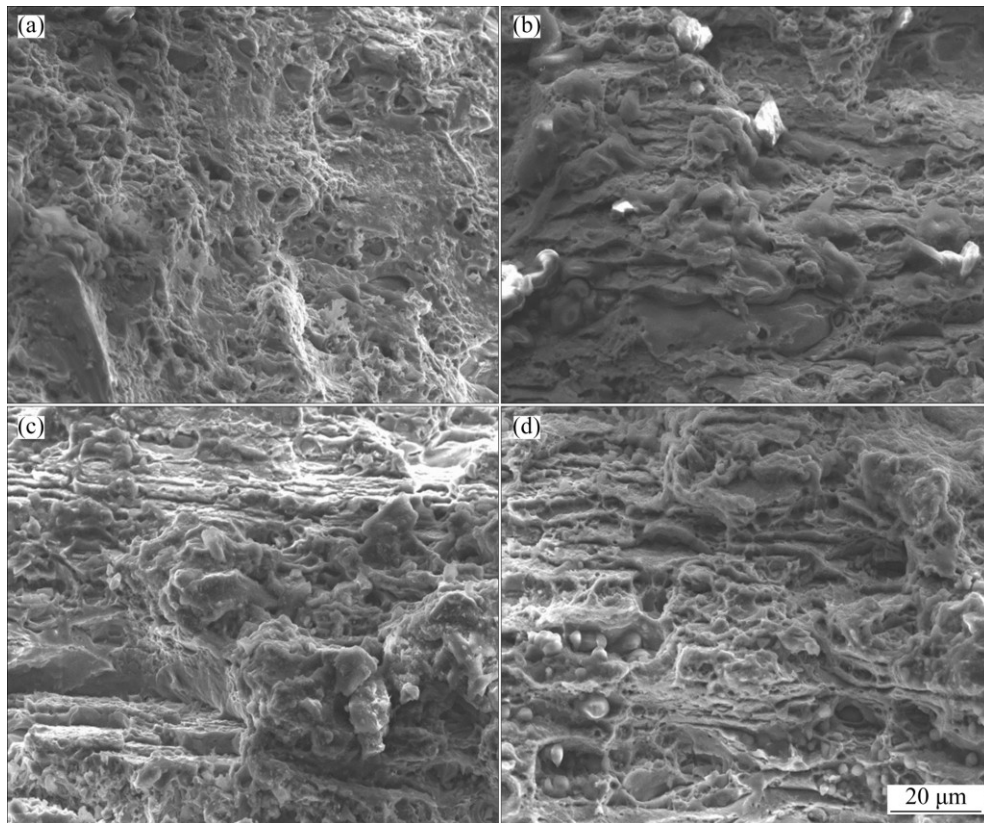


**Fig. 8** Fracture morphologies of AA2195 alloy after SSRT in air (a, c) and 3.5% NaCl solution (b, d) for longitudinal (a, b) and long transverse (c, d) directions, respectively

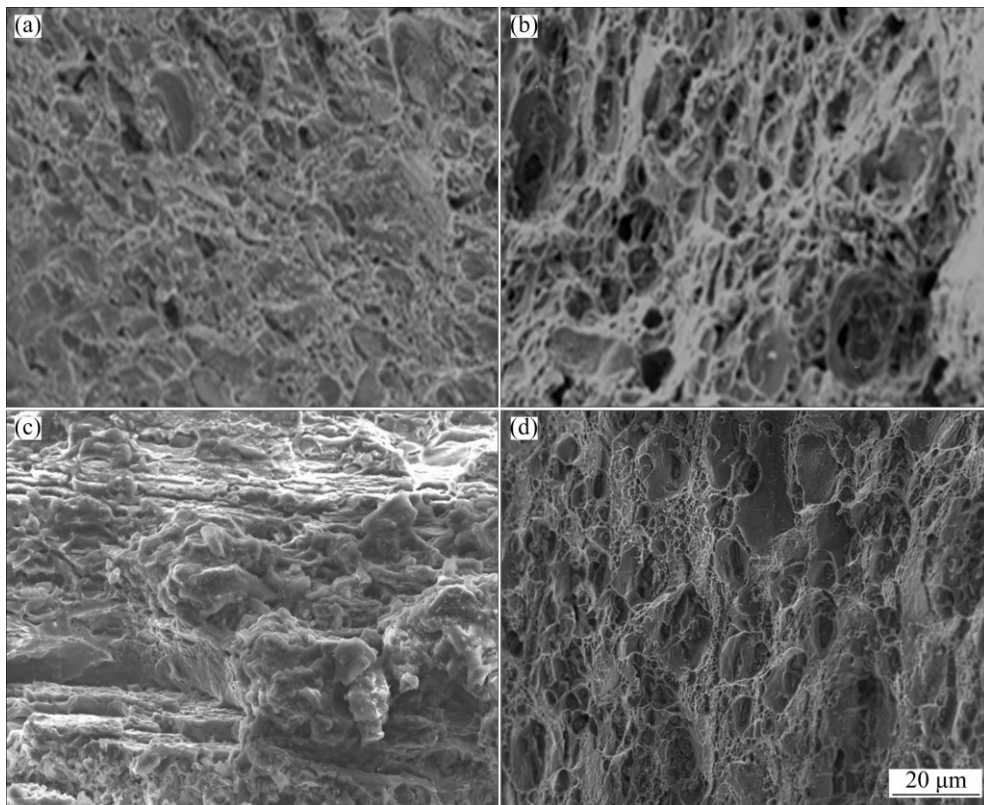


**Fig. 9** Fracture morphologies of AA2219 alloy after SSRT in air (a, c) and 3.5% NaCl solution (b, d) for longitudinal (a, b) and long transverse (c, d) directions, respectively

prior to artificial aging along with higher aging temperature used in the previous study. The high SCC susceptibility of the alloy as reported by MOSHIER et al [4] is believed to be due to fewer amount of cold working (3%) and higher aging temperature (160 °C). This view can be further confirmed from the results of WANG et al [5] who have reported predominantly IGC more of fracture for the alloy due to less cold working and higher aging temperatures. Hence, it is suggested that 7% cold working and lower aging temperature (150 °C) are essential in order to obtain good SCC resistance under the strain rate conditions used in the present study.

## 4 Conclusions

1) AA2195 alloy exhibited better general corrosion resistance than AA2219 alloy. This was due to less intensity of corrosion attack along with lower depth as measured from the non-contact optical profilometry technique.

2) The SSRT results indicate that the environmental cracking resistance of alloys AA2195 and AA2219 are comparable without any SCC susceptibility under the strain rate conditions used in the present work. The higher SCC resistances for AA2195 alloy than the earlier reported results are suggested to be due to the cold working (7%) prior to artificial aging and lower aging temperature (150 °C).

## Acknowledgment

The authors express their sincere thanks to Director, VSSC for permitting to publish the paper.

## References

- [1] DURSUN T, SOUTIS C. Recent developments in advanced aircraft aluminum alloys [J]. *Materials and Design*, 2014, 56: 862–871.
- [2] LIU Q, ZHU R H, LI J F, CHEN Y L, ZHANG X H, ZHANG L, ZHENG Z Q. Microstructural evolution of Mg, Ag, and Zn micro-alloyed alloy during homogenization [J]. *Transactions of Nonferrous Metals Society of China*, 2016, 26: 607–619.
- [3] HU W S, MELETIS E I. Corrosion and environment cracking behaviour of friction stir welded Al2195 and Al2219 alloys [J]. *Materials Science Forum*, 2000, 331–337: 1683–1688.
- [4] MOSHIER W C, SHAW B A, TACK W T, PHULL B. Stress corrosion cracking behaviour of two high-strength Al-xCu-Li-Ag-Mg-Zr alloys [J]. *Corrosion*, 1992, 48: 306–308.
- [5] WANG Xue-hui, WANG Ji-hui, XIN Yue, YUN Gao. Effect of aging treatment on the exfoliation corrosion and stress corrosion cracking behaviors of 2195 Al-Li alloy [J]. *Materials and Design*, 2015, 67: 596–605.
- [6] NAYAN N, MURTY S, JHA A K, PANT B, SHARMA S, GEORGE K M. Processing and characterization of Al-Cu-Li alloy AA2195 undergoing scale up production through the vacuum induction melting technique [J]. *Materials Science and Engineering A*, 2013, 576: 21–28.
- [7] NAYAN N, MURTY S, SHARMA S, SREEKUMAR K, SINHA P. Processing and characterization of Al-Cu-Li alloy AA2195 [J]. *Materials Science Forum*, 2012, 710: 119–124.
- [8] NAYAN N, NAIR K S, MITTAL M, SUDHAKARAN K. Studies on Al-Cu-Li-Mg-Ag-Zr alloy processed through vacuum induction melting (VIM) technique [J]. *Materials Science and Engineering A*, 2007, 454: 500–507.
- [9] HEKMAT-ARDAKAN A, ELGALLAD E M, AJERSCH F, CHEN X G. Microstructural evolution and mechanical properties of as-cast and T6-treated AA2195 DC cast alloy [J]. *Materials Science and Engineering A*, 2012, 558: 76–81.
- [10] FONDA R W, BINGERT J F. Precipitation and grain refinement in a 2195Al friction stir weld [J]. *Metallurgical and Materials Transaction A*, 2006, 37: 3593–3604.
- [11] LI J F, LIU P L, CHEN Y L, ZHANG X H, ZHENG Z Q. Microstructure and mechanical properties of Mg, Ag and Zn multi-microalloyed Al-(3.2–3.8)Cu-(1.0–1.4)Li alloys [J]. *Transactions of Nonferrous Metals Society of China*, 2015, 25: 2103–2112.
- [12] GAO C, LUAN Y, YU J C, MA Y. Effect of thermo-mechanical treatment process on microstructure and mechanical properties of 2A97 Al-Li alloy [J]. *Transactions of Nonferrous Metals Society of China*, 2014, 24: 2196–2202.
- [13] QIN Hai-long, ZHANG Hua, WU Hui-qiang. The evolution of precipitation and microstructure in friction stir welded 2195-T8 Al-Li alloy [J]. *Materials Science and Engineering A*, 2015, 626: 322–329.
- [14] DU Y X, ZHANG X M, YE L Y, LIU S D. Evolution of grain structure in AA2195 Al-Li alloy plate during recrystallization [J]. *Transactions of Nonferrous Metals Society of China*, 2006, 16: 321–326.
- [15] NAYAN N, GURAO P N, MURTY S, JHA A K, PANT B, SHARMA S, GEORGE K M. Microstructure and micro-texture evolution during large strain deformation of an aluminum-copper-lithium alloy AA2195 [J]. *Materials and Design*, 2015, 65: 862–868.
- [16] WALL F D, STONER G E. The evaluation of the critical electrochemical potentials influencing environmentally assisted cracking of Al-Cu-Li alloys in selected environments [J]. *Corrosion Science*, 1997, 39: 835–853.
- [17] MORETO J A, MARINO C E B, BOSE FILHO W W, ROCHA L A, FERNANDES J C S. SVET, SKP and EIS study of the corrosion behaviour of high strength Al and Al-Li alloys used in aircraft fabrication [J]. *Corrosion Science*, 2014, 84: 30–41.
- [18] SZKLARSKA-SMIALOWSKA Z. Pitting corrosion of aluminium [J]. *Corrosion Science*, 1999, 41: 1743–1767.
- [19] NAYAN N, MURTY S, JHA A K, PANT B, SHARMA S, GEORGE K M, SASTRY G V S. Mechanical properties of aluminum-copper-lithium alloy AA2195 at cryogenic temperatures [J]. *Materials and Design*, 2014, 58: 445–450.
- [20] LI J F, QIAO Z Z, NA J, YU T C. Localized corrosion mechanism of 2xxx series Al alloy containing  $S(Al_2CuMg)$  and  $(Al_2Cu)$  precipitates in 4.0% NaCl solution at pH 6.1 [J]. *Materials Chemistry and Physics*, 2005, 91: 325–329.
- [21] STARKE E A, STALEY J T. Application of modern aluminum alloys to aircraft [J]. *Progress in Aerospace Sciences*, 1996, 32: 131–172.
- [22] DORWARD R, PRITCHETT T. Advanced aluminum alloys for aircraft and aerospace applications [J]. *Materials and Design*, 1988, 9: 63–69.

## Al–Cu–Li 合金 AA2195 在低应变速率和 3.5% NaCl 溶液中的抗裂性能

R. GHOSH, A. VENUGOPAL, P. RAMESH NARAYANAN, S. C. SHARMA, P. V. VENKITAKRISHNAN

Materials and Metallurgy Group, Materials and Mechanical Entity,  
Vikram Sarabhai Space Centre, Thiruvananthapuram-695022, Kerala, India

**摘 要:** 研究 Al–Cu–Li 合金 AA2195 在 3.5% NaCl 环境中的耐蚀和抗裂性能, 并将其与另一高强合金 AA2219 进行比较。采用浸泡腐蚀和恒电位极化实验测定合金的总耐蚀性能; 采用低应变速率测试法确定合金的应力腐蚀开裂(SCC)性能。利用 SEM–EDS 和光学测量技术对合金样品进行表征以研究其腐蚀形貌、元素含量和腐蚀深度的变化。用韧性的减少量作为估算合金应力腐蚀开裂(SCC)敏感性的一个参数。结果表明, 由于较低的腐蚀速率、较小的腐蚀深度和宽度, AA2195 合金比 AA2219 合金具有更好的耐蚀性能。然而, 两种合金的 SCC 参数( $\epsilon_{\text{NaCl}}/\epsilon_{\text{air}}$ )均大于 0.90, 说明此两种合金均具有较好的抗裂性能。断裂样品的 SEM–EDS 结果表明, 两种合金均为典型的脆性断裂形貌。

**关键词:** Al–Cu–Li 合金; 应力腐蚀开裂; 断口形貌; 动电位极化

(Edited by Wei-ping CHEN)